Topological Inverse Band Theory in Waveguide Quantum Electrodynamics

Yongguan Ke,[1,2,3] Jiaxuan Huang,[3] Wenjie Liu,[3,4] Yuri Kivshar,[5,6,*] and Chaohong Lee[1,2,4,5,†]

[1]*Institute of Quantum Precision Measurement, State Key Laboratory of Radio Frequency Heterogeneous Integration, Shenzhen University, Shenzhen 518060, China*

[2]*College of Physics and Optoelectronic Engineering, Shenzhen University, Shenzhen 518060, China*

[3]*Laboratory of Quantum Engineering and Quantum Metrology, School of Physics and Astronomy, Sun Yat-Sen University (Zhuhai Campus), Zhuhai 519082, China*

[4]*Quantum Science Center of Guangdong-Hongkong-Macao Greater Bay Area (Guangdong), Shenzhen 518045, China*

[5]*Nonlinear Physics Center, Research School of Physics, Australian National University, Canberra, Australian Capital Territory 2601, Australia*

[6]*Qingdao Innovation and Development Center, Harbin Engineering University, Qingdao 266000, China*

(Received 15 March 2023; accepted 21 August 2023; published 8 September 2023)

Topological phases play a crucial role in the fundamental physics of light-matter interaction and emerging applications of quantum technologies. However, the topological band theory of waveguide QED systems is known to break down, because the energy bands become disconnected. Here, we introduce a concept of the inverse energy band and explore analytically topological scattering in a waveguide with an array of quantum emitters. We uncover a rich structure of topological phase transitions, symmetric scale-free localization, completely flat bands, and the corresponding dark Wannier states. Although bulk-edge correspondence is partially broken because of radiative decay, we prove analytically that the scale-free localized states are distributed in a single inverse energy band in the topological phase and in two inverse bands in the trivial phase. Surprisingly, the winding number of the scattering textures depends on both the topological phase of inverse subradiant band and the odevity of the cell number. Our Letter uncovers the field of the topological inverse bands, and it brings a novel vision to topological phases in light-matter interactions.

DOI: 10.1103/PhysRevLett.131.103604

Introduction.—Light-matter interaction plays a crucial role in the fundamental sciences [1,2], and it underpins the rapid progress of quantum technologies. Understanding intrinsic mechanisms of absorption as well as spontaneous and stimulated emissions leads to the development of practical applications, such as solar cells, light-emitting diodes, and lasers [3]. Introducing topology into light-matter interaction could bring new advances, such as topological lasers [4–7], in which monochromaticity, efficiency, and emission stability become superior to those observed for conventional lasers. To unleash the power of topology in light-matter interaction [8], it is important to understand the role of topological phases at the microscopic level of quantum electrodynamics (QED).

Waveguide QED studies photons propagating in waveguides, excitation of quantum emitters, and strong interaction between them [9–12], providing an excellent platform to explore the interplay between topology and light-matter interaction [13–26]. We notice that the previous studies are based on the well-established topological band theory, allowing one to calculate topological phases and topological invariants [27,28]. However, in waveguide QED the energy band splits into two disconnected polariton branches [29], which hinders the straightforward application of the topological band theory. It is urged to develop a new theoretical approach to explore topological phase in waveguide QED. Moreover, we need to answer how the bulk topological phase or topological invariant is imprinted in photonic scattering.

Here, we suggest and implement the topological inverse energy band theory based on a proof-of-principle waveguide QED with inversion symmetry, as depicted in Fig. 1, and we uncover a connection between topological phases and photonic scattering. We find *analytically* unexpected rich topological phase transitions driven by the spatial structure and resonant frequency of emitters. We also obtain analytically the resonant frequencies that favor a completely flat band and a group of dark Wannier states equally occupying two emitters. While the bulk-edge correspondence is partially broken due to radiative decay, we analytically prove that scale-free localized states can exist in only one inverse band in topological nontrivial phases and in two inverse bands in trivial phases. We use the reflection and transmission coefficients to construct scattering textures, which are winding as the photonic frequency is swept along an inverse subradiant band. Importantly, the winding number of scattering depends on both the topological phase of the inverse band and

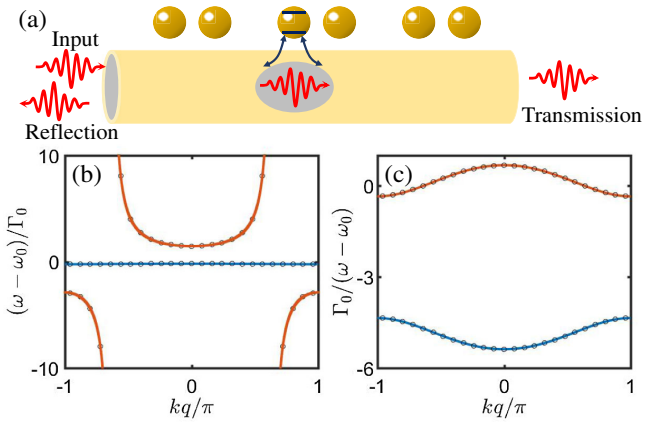

FIG. 1. Schematic diagram of photonic scattering and inverse energy band. (a) Diagram of photon in a waveguide scattered by quantum emitters. The emitter positions are arranged as $z_j = d[j + \delta\cos(\pi j + \theta)]$ with the averaged spacing d, the modulation strength δ, and the modulation phase θ. (b) Energy band. (c) Inverse energy band. The red and blue inverse energy bands originate from the red and blue bands, respectively. The black circles denote the non-Markov cases in 25 cells. The parameters are chosen as $\delta = 0.4$, $\theta = 0$, and $\varphi = 1$.

odevity of the cell number. We believe our Letter opens a field of topological inverse band theory, it provides new insights into the role of topological phases imprinted in light-matter interaction, and it paves a way to engineer the dark states for quantum information storage and precision frequency measurements.

Waveguide QED with inversion symmetry.—As a proof-of-principle example, we consider an array of quantum emitters in a photonic waveguide. The quantum emitters are two-level systems with resonant frequency ω_0 and positions arranged as $z_j = d[j + \delta\cos(2\pi/qj + \theta)]$; see Fig. 1(a). Here, each unit cell contains $q = 2$ emitters, d is the spacing constant, and δ and θ are the modulation strength and phase, respectively. The basic process is that the photon is absorbed by emitters and transferred to an excitation, which can be reversely transferred into a photon. The motion of an excitation is described by an effective Hamiltonian [30,31]

$$H_{\text{eff}} = \sum_{j=1}^{2N} \hbar\omega_0 b_j^\dagger b_j - i\hbar\Gamma_0 \sum_{j,l=1}^{2N} b_j^\dagger b_l e^{i\varphi|z_l - z_j|/d}. \quad (1)$$

Here, N is the number of cells, and the scaled Planck constant $\hbar$ is set as a unit in the following. $\Gamma_0 = g^2/c$ is the radiative decay rate of a single emitter with g denoting the coupling strength between excitation and photon and c being the velocity of light. The hopping of excitation from any two emitters is assisted by emission and reabsorption of a photon in the waveguide. The hopping strength is an infinite range with a phase shift, in which the phase unit $\varphi = \omega d/c$ depends on the injected photonic frequency ω. When the spacing constant is small enough $[d \ll c/(\omega - \omega_0)/N \sim \lambda/(2\pi N)]$, one may take the Markov approximation by replacing the phase constant with $\varphi = \omega_0 d/c$ [30].

By applying the Bloch theorem, we can immediately obtain the Hamiltonian in momentum space H_k and the Bloch states $|\psi_{n,k}\rangle = \sum_{j,l} e^{ikqj} u_{n,k}(l)|qj + l\rangle$ with energy $\omega_{n,k}$ (see Supplemental Material [31]). We find that the energy band is diverged at $k = \pm\varphi$ and is split into upper and lower polariton branches; see Fig. 1(b). The divergence of the energy band originates from the infinite-range coupling in the Markov approximation. When considering the non-Markov case in a small system with $N = 25$ cells, there is no divergence in the non-Markov energy bands [31]; see the black circles in Fig. 1(b). However, the disconnection of energy bands in both Markov and non-Markov cases hinders the application of topological band theory. To avoid the disconnection, we define the inverse energy band as

$$\bar{\omega}_k = (\omega_k - \omega_0)^{-1}, \quad (2)$$

which can be obtained by solving $H_k^{-1}|\bar{u}_{n,k}\rangle = \Gamma_0\bar{\omega}_{n,k}|\bar{u}_{n,k}\rangle$. Here, the amplitudes of state $|\bar{u}_{n,k}\rangle$ are given by $\bar{u}_{n,k}(l)$, which are the same as $u_{n,k}(l)$ if n and $\bar{n}$ are one-to-one correspondence. The inverse energy band glues the upper and lower polariton branches and becomes a continuous function; see solid lines for Markov case and black circles for the non-Markov case in Fig. 1(c). By fixing the disconnection problem, we can easily define topological phases and topological invariants based on the inverse band as usual. We find that the energy bands, the inverse energy bands, and the topological phase in Markov and non-Markov cases are consistent with each other [31]. Although the Hamiltonian and its inversion share the same eigenstates, they have different band indices and thus the inverse energy band may uncover novel topological states that are failed to be found by the original energy band.

Topological phase transition, partial breakdown of bulk-edge correspondence, and dark Wannier states.—Since the effective Hamiltonian has the inversion symmetry $H(i,j) = H(2N+1-i, 2N+1-j)$, the Zak phase [46], as a geometrical phase picked up by a particle sweeping the Brillouin zone, is quantized. The Zak phase of the nth inverse band is given by

$$\gamma = i\int_{-\pi/2}^{+\pi/2} \langle\bar{u}_{n,k}|\frac{\partial}{\partial k}|\bar{u}_{n,k}\rangle dk. \quad (3)$$

Figure 2(a) shows the Zak phase as a function of the modulation phase and the hopping phase constant. Surprisingly, the topological phase diagram is unexpectedly rich, with a nontrivial phase $\gamma = \pi$ for yellow regions and a trivial phase $\gamma = 0$ for white regions. The red lines and the black dashed lines mark the topological phase boundaries and the parameters for the flat band with energy

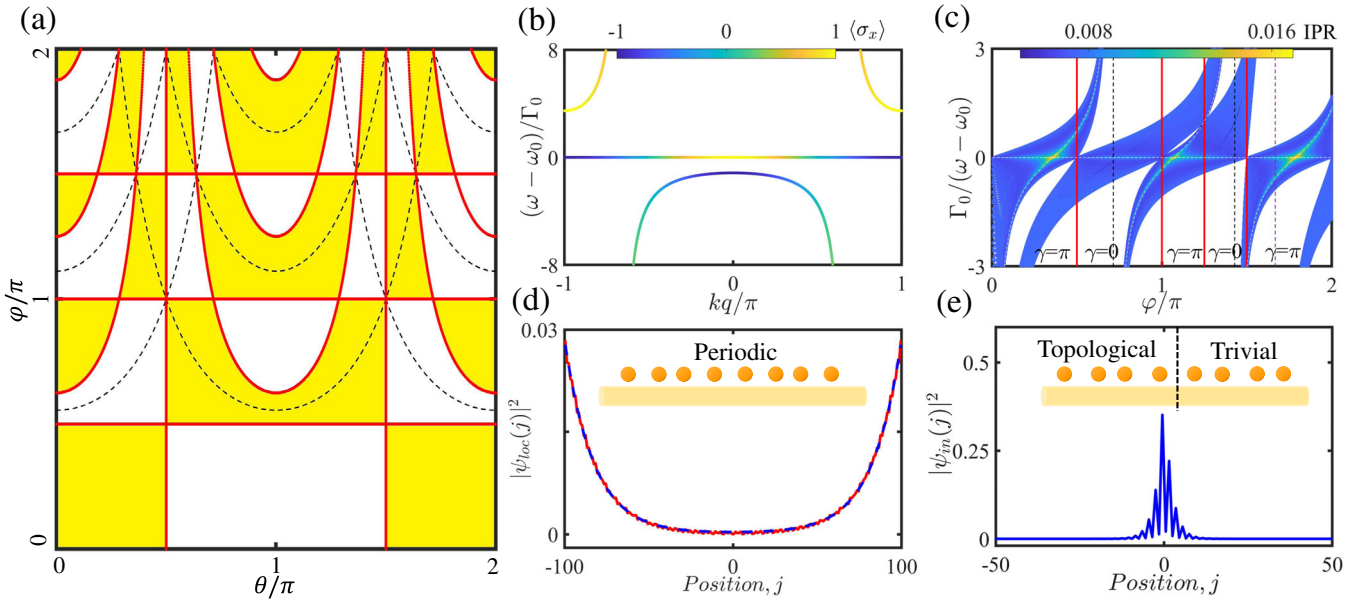

FIG. 2. Topological phase transition, breakdown of bulk-edge correspondence, and topological flat band. (a) Topological phase diagram where the white and yellow regions are trivial and topological phases, respectively. Black dashed lines denote the positions of flat bands. (b) Flat energy band with $\theta = \pi/3$ and $\varphi = 5\pi/3$. The colors denote $\langle\sigma_x\rangle$ of the corresponding eigenstates. $\langle\sigma_x\rangle$ are opposite at the high symmetry points, indicating topological phase. (c) The inverse participation ratio of $N = 100$ cells under open boundary conditions with $\theta = \pi/3$. There is no edge state at the inverse band gap. White dashed lines denote the centered inverse energy of scale-free localized states. (d) Symmetric scale-free localized states with the largest IPR (red solid line) and the fitting function $|\psi_{\rm loc}(j)|^2 \sim (e^{-\alpha j/N} + e^{\alpha j/N})^2$ (blue dashed line). The other parameters are chosen as $\theta = \pi/3$ and $\varphi = \pi/3$. (e) Topological interface state in a structure spliced by two arrays with different modulation phases $\theta = \pi/3$ and $\theta = 2\pi/3$. The above calculations are performed with modulation strength $\delta = 0.4$.

$\omega = \omega_0$ [31]. When a flat band with energy $\omega = \omega_0$ exists, because its inverse band becomes divergent, we have to combine the energy band to extract its topological phase; see Fig. 2(b) for the topological case with $\delta = 0.4$, $\theta = \pi/3$, and $\varphi = 5\pi/3$. For the continuous flat band, $\langle\sigma_x\rangle = \langle u_{n,k}|\sigma_x|u_{n,k}\rangle$ changes from -1 at $k = \pi/2$ to 1 at $k = 0$, where σ_x is the Pauli matrix. The sign difference of $\langle\sigma_x\rangle$ between high symmetric points is related to the Zak phase, similar to Ref. [47]. For a fixed spatial structure, we can drive the topological phase transition by the resonant frequency ($\varphi = \omega_0/cd$), which can be controlled by either the resonant frequency of an injected photon or the Zeeman shift induced by magnetic fields. This is in stark contrast to the topological phases in electronic materials, which are largely determined by the crystal structure.

To explore the bulk-edge correspondence, we calculate the inverse participation ratio (IPR) of eigenstates in a finite array under open boundary conditions, IPR $= \sum |\psi_n(j)|^4$, where $\psi_n(j)$ is the amplitude of the nth eigenstate at the jth site. The IPR tends to 1 for the most localized state and 0 for the extended state, which can be used to distinguish localized and extended states. Figure 2(c) shows the dependence of IPRs on the hopping phase constant and the inverse energy. The red solid lines separate the energy spectrum into several regions with different Zak phases. There are no edge modes in the inverse band gaps, regardless of trivial or topological phases. The breakdown of the conventional bulk-edge correspondence can be explained by the inverse of the effective Hamiltonian, which turns out to be a Su-Schrieffer-Heeger model with effective radiative defects at the boundaries (see Supplemental Material [31]). It immediately becomes clear that an excitation at the end sites may well escape away from the system of emitters as a propagating photon.

However, the bulk topological phase still has significant consequences. First, symmetric scale-free localized states [Fig. 2(d)], $|\psi_{\rm loc}(j)|^2 \sim (e^{-\alpha j/N} + e^{\alpha j/N})^2$, exist in the continuous spectrum with larger IPRs [31–33]. Surprisingly, the distribution of scale-free localized states in inverse energy bands depends on topological properties; see Fig. 2(c). In the topological phase with $\gamma = \pi$, the scale-free localized states can be distributed in only one single inverse energy band; in the trivial phase with $\gamma = 0$, they can be distributed in both two inverse energy bands. We analytically prove this observation and obtain the centered inverse energy of the scale-free localized states denoted by the white dashed lines in Fig. 2(c) [31]. Second, the number (S) of subradiant states in the energy band around ω_0 is $S = N$ for a trivial phase and $S = N - 1$ for a topological phase. These subradiant states become dark states when the band becomes completely flat with energy $\omega = \omega_0$ [31]. Because the flat band has zero group velocity and infinite effective mass, the lifetime of

excitation can be infinitely long. In the flat band, we find N dark Wannier states being intercell superposition $(|2j-1\rangle + |2j\rangle)/\sqrt{2}$ $(j=1,2,\ldots,N)$ in the trivial phase and $N-1$ dark Wannier states being intracell superposition $(|2j\rangle + |2j+1\rangle)/\sqrt{2}$ $(j=1,2,\ldots,N-1)$ in the topological phase. These dark Wannier states form a decoherence-free subspace, which is simple, arranged in order, and with the same energy of resonant frequency ω_0. These features could potentially be used for quantum memory, quantum information process, and precision frequency measurement [31]. Third, we can further extract the Zak phase of the inverse energy band via long-time average of mean cell position in quantum walks [31,34,35].

We need to emphasize that the radiative defects at the boundaries only partially break the bulk-edge correspondence. In a splicing structure that connects two arrays with different Zak phases, we find topological interface states [Fig. 2(e)] appearing in the inverse energy gaps. Because of no radiative defects at the interface, the topological interface states in large inverse energy gaps are immune to disorder to some extent. In contrast to the topological materials, in the hybrid quantum waveguide QED systems the bulk-edge correspondence is preserved in the interface between two arrays, but fails in the interface between an array and a vacuum.

Bulk topology of photonic scattering.—Because an excitation will generally decay into a photon in the long-time dynamics, it is highly appealing to explore how the topology of excitation is mapped to the topology of photonic scattering. We consider a photon with momentum (κ) injected into the waveguide. After interacting with the emitters and transferring into excitation, or vice versa, the photon is either reflected or transmitted. The reflection and transmission coefficients are given by

$$r_\kappa = -i\Gamma_0 \sum_{j,j'} G_{j,j'}(\omega_\kappa) e^{i\omega_\kappa/c(z_j+z_{j'})}, \tag{4}$$

and

$$t_\kappa = 1 - i\Gamma_0 \sum_{j,j'} G_{j,j'}(\omega_\kappa) e^{i\omega_\kappa/c(z_{j'}-z_j)}, \tag{5}$$

which satisfy $|r_\kappa|^2 + |t_\kappa|^2 = 1$ [31]. Here, $G(\omega) = (\omega - H_{\text{eff}})^{-1}$ is the Green's function for an excitation. We calculate the reflection spectrum as a function of the inverse energy for the cases of topological nontrivial and trivial phases; see Figs. 3(a) and 3(c), respectively. When the photonic frequency is in resonance with the subradiant states, the photon is completely transmitted, and there are $N-1$ (N) dips for the topological nontrivial (trivial) phase in the shadow regions where the photonic frequency sweeps across the lower inverse band.

To show how the topological phase affects the scattering, we need to calculate the scattering textures $s_i = \langle\psi_\kappa|\sigma_i|\psi_\kappa\rangle$ $(i=x,y,z)$, where $\{|\psi_\kappa\rangle = (r_\kappa, t_\kappa)^T\}$ and σ_i are Pauli matrices. The scattering textures can potentially be probed by interference between reflected and transmitted photons. With the scattering textures $\vec{\mathbf{s}} = (s_x, s_y, s_z)$, we can define the winding number of scattering along the $x(y)$ direction as

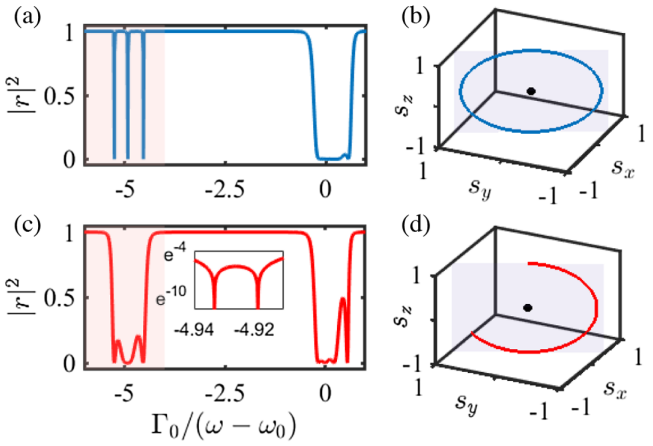

FIG. 3. Topology-dependent scattering in four cells. (a),(c) Reflection as a function of inverse energy in topological and trivial phases, respectively. The inset of (d) enlarges its region with two nearby dips. There are $N(N-1)$ dips in reflection spectrum around the subradiant inverse energy band for trivial (topological) phase. (b),(d) The trajectory of (s_x, s_y, s_z) as the inverse energy sweeps through the shading regions for topological and trivial phases, respectively. The parameters are chosen as $N=4$, $\delta=0.4$, $g=1$, $\Gamma_0=0.01$, $\omega_0=c/d=100$, $\theta=0$, and $\theta=\pi$ for topological and trivial phases, respectively.

$$\nu_{x(y)} = \int \left[\vec{\mathbf{s}} \times \frac{\partial \vec{\mathbf{s}}}{\partial \bar{\omega}}\right]_{x(y)} d\bar{\omega}, \tag{6}$$

where $\bar{\omega}$ sweeps through the lower inverse band. However, $\nu_{x(y)}$ is generally not quantized along the $x(y)$ directions. As the trajectories (s_x, s_y, s_z) in Figs. 3(b) and 3(d) locate in a plane parallel to the z direction and depart from both the x and y directions, we can define a winding number around the original point and along the direction perpendicular to the plane as

$$\nu = \sqrt{\nu_x^2 + \nu_y^2}. \tag{7}$$

We summarize the winding number in different topological phases with even and odd cells; see Table I. Remarkably, the winding number of the scattering textures depends on both the topological phase and the odevity of the cell numbers. We numerically find that a subradiant state contributes a π phase shift (see Supplemental Material [31]). Based upon the fact that there are $(N-1)$ subradiant states in a topological phase and N subradiant states in a trivial phase, we can reasonably argue that both the topological nontrivial

TABLE I. Winding number for the trajectory of scattering textures (see Supplemental Material [31]).

	Topological nontrivial	Topological trivial
Even cell	1	0
Odd cell	0	1

phase with even cells and the trivial phase with odd cells contribute π phase to the scattering texture, leading to nontrivial quantization of winding number ν.

Topological interface state in transmission spectrum.—A topological interface state exists in the structure spliced by two arrays with different topological properties. Because the topological interface state is a subradiant state, it will enhance the transmission when an injected photon is in resonance with it. We show the transmission spectrum as a function of the modulation strength δ and the inverse frequency; see Fig. 4(a). The red dashed line denotes the inverse frequency of the topological interface state in the inverse band gap, at which the transmission is strongly enhanced. At a small modulation strength $\delta = 0.1$, the profile of the transmission spectrum becomes an asymmetric Fano resonance around the topological interface state [48,49]. The Fano resonance is an interplay between the topological interface state and the states close to the inverse band edge.

Discussion.—Since the inverse energy band is related to the inverse of the Hamiltonian known as Green's function, the topological inverse energy band actually reflects the topological phase of Green's function, which is directly related to the scattering of a photon. It means that the topological inverse band could be a powerful and natural theoretical framework for predicting and tailoring novel topological-enriched light-matter interactions. We expect an unexplored richness in topological QED within the topological inverse band theory, considering higher dimensions that favor a variety of symmetries [24,50], more photons that support stimulated emission, quantum correlations and entanglement [17], and cavity-mediated long-range interactions [51–53].

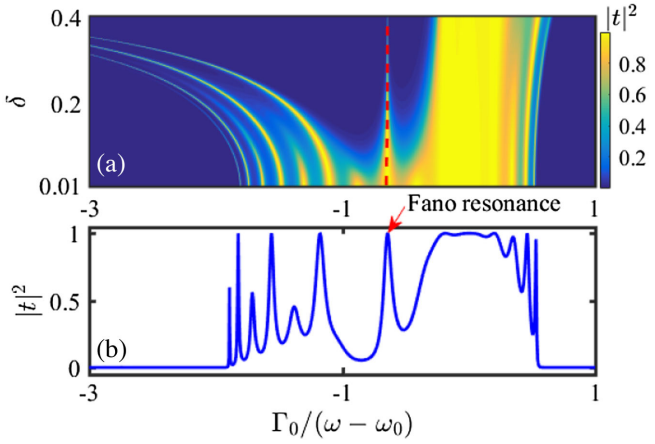

FIG. 4. (a) Transmission enhanced by topological interface state and (b) Fano resonance due to the topological interface state in the case of $\delta = 0.1$. The parameters are chosen as $N = 8$, $g = 1$, $\Gamma_0 = 0.01$, $\omega_0 = c/d = 100$. The modulation phases of the two connecting arrays are given by $\theta = 0$ and $\theta = \pi$.

We acknowledge useful discussions with Alexander Poddubny, Ling Lin, Li Zhang, and Linhu Li. This work is supported by the National Key Research and Development Program of China (Grant No. 2022YFA1404104), the National Natural Science Foundation of China (Grants No. 12025509 and No. 12275365), the Key-Area Research and Development Program of Guangdong Province (Grant No. 2019B030330001), and the Natural Science Foundation of Guangdong Province (Grant No. 2023A1515012099). Y. Kivshar is supported by the Australian Research Council (Grants No. DP200101168 and No. DP210101292).

*Corresponding author: yuri.kivshar@anu.edu.au
†Corresponding author: chleecn@szu.edu.cn; chleecn@gmail.com

[1] P. Forn-Díaz, L. Lamata, E. Rico, J. Kono, and E. Solano, Ultrastrong coupling regimes of light-matter interaction, Rev. Mod. Phys. **91**, 025005 (2019).
[2] R. Gutzler, M. Garg, C. R. Ast, K. Kuhnke, and K. Kern, Light–matter interaction at atomic scales, Nat. Rev. Phys. **3**, 441 (2021).
[3] C. Cohen-Tannoudji, J. Dupont-Roc, and G. Grynberg, Atom–photon interactions: Basic process and applications, in *Atom–Photon Interactions: Basic Process and Applications* (John Wiley & Sons, Ltd., New York, 1998), Chap. 2, pp. 67–163.
[4] P. St-Jean, V. Goblot, E. Galopin, A. Lemaître, T. Ozawa, L. Le Gratiet, I. Sagnes, J. Bloch, and A. Amo, Lasing in topological edge states of a one-dimensional lattice, Nat. Photonics **11**, 651 (2017).
[5] M. A. Bandres, S. Wittek, G. Harari, M. Parto, J. Ren, M. Segev, D. N. Christodoulides, and M. Khajavikhan, Topological insulator laser: Experiments, Science **359**, eaar4005 (2018).
[6] G. Harari, M. A. Bandres, Y. Lumer, M. C. Rechtsman, Y. D. Chong, M. Khajavikhan, D. N. Christodoulides, and M. Segev, Topological insulator laser: Theory, Science **359**, eaar4003 (2018).
[7] H.-R. Kim, M.-S. Hwang, D. Smirnova, K.-Y. Jeong, Y. Kivshar, and H.-G. Park, Multipolar lasing modes from topological corner states, Nat. Commun. **11**, 5758 (2020).
[8] S. Kruk, A. Poddubny, D. Smirnova, L. Wang, A. Slobozhanyuk, A. Shorokhov, I. Kravchenko, B. Luther-Davies, and Y. Kivshar, Nonlinear light generation in topological nanostructures, Nat. Nanotechnol. **14**, 126 (2019).
[9] P. Lodahl, S. Mahmoodian, and S. Stobbe, Interfacing single photons and single quantum dots with photonic nanostructures, Rev. Mod. Phys. **87**, 347 (2015).

[10] D. Roy, C. M. Wilson, and O. Firstenberg, Colloquium: Strongly interacting photons in one-dimensional continuum, Rev. Mod. Phys. **89**, 021001 (2017).
[11] D. E. Chang, J. S. Douglas, A. González-Tudela, C.-L. Hung, and H. J. Kimble, Colloquium: Quantum matter built from nanoscopic lattices of atoms and photons, Rev. Mod. Phys. **90**, 031002 (2018).
[12] A. S. Sheremet, M. I. Petrov, I. V. Iorsh, A. V. Poshakinskiy, and A. N. Poddubny, Waveguide quantum electrodynamics: Collective radiance and photon-photon correlations, Rev. Mod. Phys. **95**, 015002 (2023).
[13] S. Barik, A. Karasahin, C. Flower, T. Cai, H. Miyake, W. DeGottardi, M. Hafezi, and E. Waks, A topological quantum optics interface, Science **359**, 666 (2018).
[14] M. Bello, G. Platero, J. I. Cirac, and A. González-Tudela, Unconventional quantum optics in topological waveguide QED, Sci. Adv. **5**, eaaw0297 (2019).
[15] C. A. Downing, T. J. Sturges, G. Weick, M. Stobińska, and L. Martín-Moreno, Topological Phases of Polaritons in a Cavity Waveguide, Phys. Rev. Lett. **123**, 217401 (2019).
[16] L. Wang, L. Yuan, X. Chen, and S. Fan, Single-Photon Transport in a Topological Waveguide from a Dynamically Modulated Photonic System, Phys. Rev. Appl. **14**, 014063 (2020).
[17] Y. Ke, J. Zhong, A. V. Poshakinskiy, Y. S. Kivshar, A. N. Poddubny, and C. Lee, Radiative topological biphoton states in modulated qubit arrays, Phys. Rev. Res. **2**, 033190 (2020).
[18] H. Cai and D.-W. Wang, Topological phases of quantized light, Natl. Sci. Rev. **8**, nwaa196 (2020).
[19] J. Perczel, J. Borregaard, D. E. Chang, S. F. Yelin, and M. D. Lukin, Topological Quantum Optics Using Atomlike Emitter Arrays Coupled to Photonic Crystals, Phys. Rev. Lett. **124**, 083603 (2020).
[20] A. V. Poshakinskiy, J. Zhong, Y. Ke, N. A. Olekhno, C. Lee, Y. S. Kivshar, and A. N. Poddubny, Quantum Hall phases emerging from atom–photon interactions, npj Quantum Inf. **7**, 34 (2021).
[21] L. Leonforte, A. Carollo, and F. Ciccarello, Vacancy-Like Dressed States in Topological Waveguide QED, Phys. Rev. Lett. **126**, 063601 (2021).
[22] W. Nie, T. Shi, F. Nori, and Y.-x. Liu, Topology-Enhanced Nonreciprocal Scattering and Photon Absorption in a Waveguide, Phys. Rev. Appl. **15**, 044041 (2021).
[23] E. Kim, X. Zhang, V. S. Ferreira, J. Banker, J. K. Iverson, A. Sipahigil, M. Bello, A. González-Tudela, M. Mirhosseini, and O. Painter, Quantum Electrodynamics in a Topological Waveguide, Phys. Rev. X **11**, 011015 (2021).
[24] D. De Bernardis, Z.-P. Cian, I. Carusotto, M. Hafezi, and P. Rabl, Light-Matter Interactions in Synthetic Magnetic Fields: Landau-Photon Polaritons, Phys. Rev. Lett. **126**, 103603 (2021).
[25] J.-S. Tang, W. Nie, L. Tang, M. Chen, X. Su, Y. Lu, F. Nori, and K. Xia, Nonreciprocal Single-Photon Band Structure, Phys. Rev. Lett. **128**, 203602 (2022).
[26] P. Jiang, N. Ma, X. Qiao, and H. Zhang, Recent progress in chiral topological quantum interface, Front. Phys. **10**, 845579 (2022).
[27] A. Bansil, H. Lin, and T. Das, Colloquium: Topological band theory, Rev. Mod. Phys. **88**, 021004 (2016).
[28] T. Ozawa, H. M. Price, A. Amo, N. Goldman, M. Hafezi, L. Lu, M. C. Rechtsman, D. Schuster, J. Simon, O. Zilberberg, and I. Carusotto, Topological photonics, Rev. Mod. Phys. **91**, 015006 (2019).
[29] Y. Marques, I. A. Shelykh, and I. V. Iorsh, Bound Photonic Pairs in 2D Waveguide Quantum Electrodynamics, Phys. Rev. Lett. **127**, 273602 (2021).
[30] Y. Ke, A. V. Poshakinskiy, C. Lee, Y. S. Kivshar, and A. N. Poddubny, Inelastic Scattering of Photon Pairs in Qubit Arrays with Subradiant States, Phys. Rev. Lett. **123**, 253601 (2019).
[31] See Supplemental Material at http://link.aps.org/supplemental/10.1103/PhysRevLett.131.103604 for details of (S1) Effective Hamiltonian for the excitation; (S2) energy band, inverse energy band, and Zak phase; (S3) topological phase boundaries; (S4) flat band and dark Wannier states; (S5) scale-free localized states; (S6) extraction of topological phase via quantum walks; (S7) Green's function method; (S8) winding number of scattering textures; (S9) phase shift due to subradiant states, which includes Refs. [30,32–45].
[32] L. Li, C. H. Lee, and J. Gong, Impurity induced scale-free localization, Commun. Phys. **4**, 42 (2021).
[33] B. Li, H.-R. Wang, F. Song, and Z. Wang, Scale-free localization and PT symmetry breaking from local non-Hermiticity, arXiv:2302.04256.
[34] S. Longhi, Probing one-dimensional topological phases in waveguide lattices with broken chiral symmetry, Opt. Lett. **43**, 4639 (2018).
[35] Z.-Q. Jiao, S. Longhi, X.-W. Wang, J. Gao, W.-H. Zhou, Y. Wang, Y.-X. Fu, L. Wang, R.-J. Ren, L.-F. Qiao, and X.-M. Jin, Experimentally Detecting Quantized Zak Phases Without Chiral Symmetry in Photonic Lattices, Phys. Rev. Lett. **127**, 147401 (2021).
[36] J.-T. Shen and S. Fan, Strongly Correlated Two-Photon Transport in a One-Dimensional Waveguide Coupled to a Two-Level System, Phys. Rev. Lett. **98**, 153003 (2007).
[37] F. Dinc, I. Ercan, and A. M. Brańczyk, Exact Markovian and non-Markovian time dynamics in waveguide QED: Collective interactions, bound states in continuum, superradiance and subradiance, Quantum **3**, 213 (2019).
[38] M. Zanner, T. Orell, C. M. Schneider, R. Albert, S. Oleschko, M. L. Juan, M. Silveri, and G. Kirchmair, Coherent control of a multi-qubit dark state in waveguide quantum electrodynamics, Nat. Phys. **18**, 538 (2022).
[39] R. Holzinger, R. Gutiérrez-Jáuregui, T. Hönigl-Decrinis, G. Kirchmair, A. Asenjo-Garcia, and H. Ritsch, Control of Localized Single- and Many-Body Dark States in Waveguide QED, Phys. Rev. Lett. **129**, 253601 (2022).
[40] V. Paulisch, H. J. Kimble, and A. González-Tudela, Universal quantum computation in waveguide QED using decoherence free subspaces, New J. Phys. **18**, 043041 (2016).
[41] D. E. Chang, J. Ye, and M. D. Lukin, Controlling dipole-dipole frequency shifts in a lattice-based optical atomic clock, Phys. Rev. A **69**, 023810 (2004).
[42] J. Ruostekoski and J. Javanainen, Arrays of strongly coupled atoms in a one-dimensional waveguide, Phys. Rev. A **96**, 033857 (2017).

[43] J. Javanainen and R. Rajapakse, Light propagation in systems involving two-dimensional atomic lattices, Phys. Rev. A **100**, 013616 (2019).
[44] S. L. Campbell, R. Hutson, G. Marti, A. Goban, N. Darkwah Oppong, R. McNally, L. Sonderhouse, J. Robinson, W. Zhang, B. Bloom *et al.*, A Fermi-degenerate three-dimensional optical lattice clock, Science **358**, 90 (2017).
[45] A. N. Poddubny, Quasiflat band enabling subradiant two-photon bound states, Phys. Rev. A **101**, 043845 (2020).
[46] J. Zak, Berry's Phase for Energy Bands in Solids, Phys. Rev. Lett. **62**, 2747 (1989).
[47] L. Fu and C. L. Kane, Topological insulators with inversion symmetry, Phys. Rev. B **76**, 045302 (2007).
[48] M. F. Limonov, M. V. Rybin, A. N. Poddubny, and Y. S. Kivshar, Fano resonances in photonics, Nat. Photonics **11**, 543 (2017).
[49] F. Zangeneh-Nejad and R. Fleury, Topological Fano Resonances, Phys. Rev. Lett. **122**, 014301 (2019).
[50] C. Vega, D. Porras, and A. González-Tudela, Topological multi-mode waveguide QED, Phys. Rev. Res. **5**, 023031 (2023).
[51] V. D. Vaidya, Y. Guo, R. M. Kroeze, K. E. Ballantine, A. J. Kollár, J. Keeling, and B. L. Lev, Tunable-Range, Photon-Mediated Atomic Interactions in Multimode Cavity QED, Phys. Rev. X **8**, 011002 (2018).
[52] T. Chanda, R. Kraus, G. Morigi, and J. Zakrzewski, Self-organized topological insulator due to cavity-mediated correlated tunneling, Quantum **5**, 501 (2021).
[53] F. Mivehvar, F. Piazza, T. Donner, and H. Ritsch, Cavity QED with quantum gases: New paradigms in many-body physics, Adv. Phys. **70**, 1 (2021).